Journal of The Electrochemical Society, **159** (2) E45-E51 (2012)
0013-4651/2012/159(2)/E45/7/$28.00 © The Electrochemical Society

High-Efficiency Electrodeposition of Large Scale ZnO Nanorod Arrays for Thin Transparent Electrodes

D. Pullini,[a] A. Pruna,[a,b,*,e,z] S. Zanin,[a,c] and D. Busquets Mataix[d]

[a] *Centro Ricerche Fiat, 10043 Orbassano (TO), Italy*
[b] *University Politehnica of Bucharest, 010737 Bucharest, Romania*
[c] *Instituto de Tecnología de Materiales and* [d] *Departamento de Ingeniería Mecánica y de Materiales, Universidad Politécnica de Valencia, Camino de Vera s/n 46022 Valencia, Spain*

In the present work an effective technique to synthesize large-scale c-axis oriented ZnO nanorod (NR) arrays is presented. The manuscript reports a single-step cathodic electrodeposition, either in aqueous and organic electrolytes, to fill up ultra-thin anodic nanoporous alumina templates. Prior to growing, self-ordered hexagonal array of cylindrical nanopores have been fabricated by anodizing Al thin films previously deposited onto ITO/glass substrates. The diameter and the aspect ratio of the vertically aligned nanopores are about 60 nm and 8:1, respectively. The results of this work demonstrate that using dimethyl sulfoxide (DMSO) as an electrolyte leads to a growth more homogeneous in shape and crystallinity, and with 60% deposition efficiency – the highest by now in literature. This fact is most probably due to a better infiltration of the alumina nanopores by this electrolyte. SEM and XRD analysis were employed for the study of morphology and crystalline structure of the obtained ZnO NR. These measurements showed furthermore that ZnO nanorod arrays are uniformly embedded into the hexagonally ordered nanopores of the anodic alumina membrane. DMSO proved to be an optimal electrolyte to obtain single-crystalline ZnO NR arrays, highly transparent in visible light range (80% transmittance).
 [DOI: 10.1149/2.093202jes]

Manuscript submitted October 3, 2011; revised manuscript received November 10, 2011. Published December 20, 2011.

In recent years, self-assembled semiconductor nanostructures have attracted much interest, since they hold promise for various applications.[1] Based on their remarkable physical properties and the motivation for device miniaturization, large effort has been focused on the synthesis, characterization and device applications of zinc oxide (ZnO) nanomaterials. ZnO has applications in optoelectronics in the ultraviolet (UV) and blue spectral region, piezoelectric devices, chemical sensors and spin electronics.[2–5] Compared with other wide gap semiconductors, ZnO has a larger extinction binding energy (60 meV), which provides more efficient excitonic emission at room temperature.

An assortment of ZnO nanostructures, such as nanowires, nanotubes or nano-tetrapods have been successfully grown via a variety of methods including chemical vapor deposition, thermal evaporation and electrodeposition.[6–8] A popular strategy of ZnO nanowire synthesis is the vapor phase method, such as the (metal-catalyzed) thermal vapor transport and sedimentation method.[9] Besides the limitations of a high preparation temperature and energy-consuming experiment facilities, these vapor-phase methods usually need expensive and/or insulating substrates, such as sapphire[10] or gallium nitride (GaN)[11] for epitaxial growth. On the contrary, solution approaches are attractive due to their low cost and high yield. Electrodeposition is a cost-effective and very powerful method to grow and tailor a large range of materials.[12–14] For preparing one-dimensional nanostructure arrays, the most direct route and an elegant approach is the template-assisted method.[15] The ordered array of pores of high aspect ratio whose dimensions can be accurately tuned by the process parameters has made porous anodic alumina template (PAA) a suitable host for the fabrication of nanowires/nanorods of a wide range of materials.[16] Ordered ZnO nanowire arrays embedded in porous anodic alumina (PAA) templates have already been fabricated by electrodepositing Zn into PAA nanopores to form metallic nanowire arrays which were further oxidized.[17]

The electrolyte has shown a marked influence on the template synthesis of ZnO. On one hand, the aqueous solution induces the deposition of $Zn(OH)_2$ competing with the formation of ZnO[18] and so, the $Zn(OH)_2$ composition can quench the near band emission of ZnO.[17] On the other hand, the non-aqueous electrolyte proved to inhibit the formation of $Zn(OH)_2$,[19,20] and therefore a higher deposition temperature could be used, leading to increased crystallinity without corking up the nanopores of the PAA in the electrodeposition process. It has been shown that in case of low energy liquids such as dimethyl sulfoxide (DMSO), the equilibrium is achieved between polar and surface tension properties for a complete filling of the porous surface.[21]

Although many efforts have been made for ZnO synthesis by template electrodepositon, it has not yet been fully exploited from an industrialization standpoint. It is still a challenge to design highly transparent electrodes based on single-crystalline ZnO nanorod arrays in order to be integrated in hybrid devices since controlling the nanowires/nanorods orientation and position during the deposition is highly important as it facilitates the subsequent fabrication processes in the design of new devices. As it is known, in conventional solar cells, greater thickness of active material means better light absorption but it also means that is more difficult for electrons to escape. Therefore, not only nanorods use is cost effective due to small amount of active material, but they also maximize light absorption and provide electrons with a defined pathway to the electrode for efficient charge collection, provided that their length is small enough as not to cause a decrease of charge collection efficiency.[22] As an ordered topology that increases the rate of electron transport, a nanorod electrode may provide a means to improve the quantum efficiency of a solar cell. Thus, controlling the nanorods geometry is a key factor for high efficient optoelectronic devices. Here is presented a one-step solution template synthesis of nanorods toward ultra-thin hybrid solar cells.

The fabrication of standing ordered ZnO nanowire arrays on transparent rigid substrates that could be incorporated in optoelectronic devices is aimed in this paper. We report the fabrication of large scale uniform c-axis oriented ZnO nanorod arrays based on ultra-thin porous alumina templates on ITO/glass substrate by one step template electrochemical deposition. The influence of electrolyte and deposition conditions on the crystallinity of ZnO NR was studied.

Materials and Methods

Substrate preparation.— Prior to the PAA fabrication, the ITO/glass substrates were degreased in Cole-Parmer Micro 90 Cleaning Solution at 50°C for 1 hour, and then cleaned successively for 15 minutes each in distilled water and isopropanol in an ultrasonic

* Electrochemical Society Active Member.
[e] Present address: Instituto de Tecnología de Materiales, Universidad Politécnica de Valencia, Camino de Vera s/n, 46022 Valencia, Spain.
[z] E-mail: apruna@itm.upv.es; ai.pruna@gmail.com

bath. For the fabrication of ultrathin alumina templates, 10 nm thick Ti and 30 nm thick W adhesion layers were sputtered on ITO in order to relieve the structural stress and to permit a slow oxidation process under the anodization conditions.[23] Further, a 500 nm layer of aluminum is provided on the substrate by electron-beam evaporation (BOC Edwards) by applying 80 mA current for 1 minute.

Porous alumina templates preparation.— The PAA templates supported on ITO/glass substrates were prepared by a two-step anodization process in 0.3 M oxalic acid electrolyte applying 40 V at 5°C. After the first step of anodization, the specimens were immersed in a mixture of 6 wt % H_3PO_4 and 1.8 wt % H_2CrO_4 to remove the alumina layer. Then, the aluminum film was anodized again under the same conditions as the first step. After aluminum was consumed, the barrier layer was removed by chemical etching in 0.3 M H_3PO_4 at 36°C for a period of time varying from 10 to 20 minutes depending on the alumina template thickness. Further, the sample was rinsed thoroughly in deionized water.

ZnO nanorod arrays synthesis.— The ZnO NR were prepared by electrodeposition using both potentiostatic method and pulsed potential method (PED) from three aqueous solutions and one organic electrolyte of different zinc salts: electrolyte A: $ZnCl_2$ in a KCl supporting electrolyte and with H_2O_2 as oxygen precursor, electrolyte B: $Zn(NO_3)_2$, electrolyte C: $Zn(NO_3)_2$ using H_3BO_3 as stabilizer and electrolyte D: the $Zn(NO_3)_2$ in DMSO. The ultrapure water was provided by a Millipore setup. A 500 AMEL potentiostat and a standard three-electrode set-up with a thermostat were used for depositions. All the deposition experiments were performed at 80°C in an electrolytic bath using convection. A saturated calomel electrode (SCE) was used as the reference electrode and a Pt plate as the counter electrode. A treatment in the ultrasonic bath for a period of 10 minutes was applied to the working electrode before all the electrodepositions performed in aqueous media in order to increase the wettability of alumina template.

Characterization methods.— The morphology of the samples was characterized employing a FEI Quanta 200 3D scanning electron microscope equipped with energy dispersive X-ray (EDAX) detector. For SEM observation, the PAA template was partially dissolved in 0.1 M NaOH solution for 3–10 minutes, depending on the template thickness. It was shown that the amorphous alumina dissolution is both thermodynamically and kinetically favored without a significant loss of ZnO NR by chemical dissolution at more alkaline pH.[24] The residual NaOH solution on the surface of the PAA template was carefully rinsed several times with deionized water. Before SEM imaging, the samples were dried in air at 100°C. X-ray diffraction spectra of the ZnO NR was obtained using a Seifert 3003 PTS diffractometer with Cu X-ray source and $\lambda = 0.15419$ nm and operating at 40 kV and 40 mA. TEM microscopy was performed with a Phillips CM-10 microscope working at 100 kV. Prior to TEM analysis, the samples were immersed in 0.1 M NaOH in order to remove the PAA template and then rinsed. For the optical measurements a Cary Varian spectrophotometer was employed. Electrical properties measurements were performed on the nanowire samples at room temperature after sputtering a 50 nm top contact layer of Au.

Results and Discussion

In the present manuscript, nanoporous films are prepared on ITO covered glass as an example for a technology-relevant rigid substrate in order to provide transparent conductive substrates for optoelectronic applications. An example of highly transparent thin template on ITO/glass substrate can be seen in Figure 1d.

A SEM micrograph of a typical surface view of the PAA template is shown in Figure 1. Figure 1a shows the PAA template before the barrier removal. As one can be observe, the PAA presents dark areas with a regular pattern of an average diameter of 45 nm representing the pores and surrounding areas of aluminum oxide.

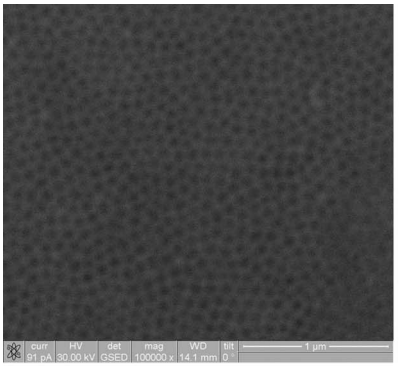

(a)

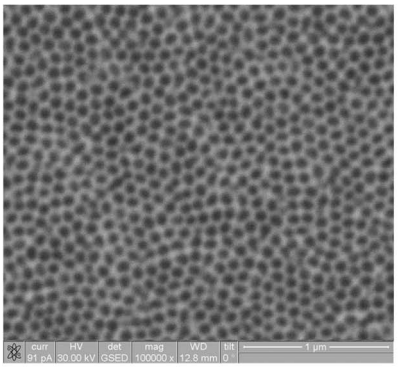

(b)

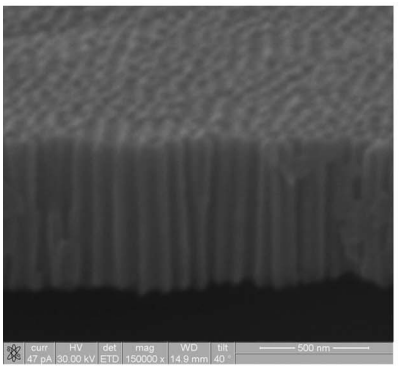

(c)

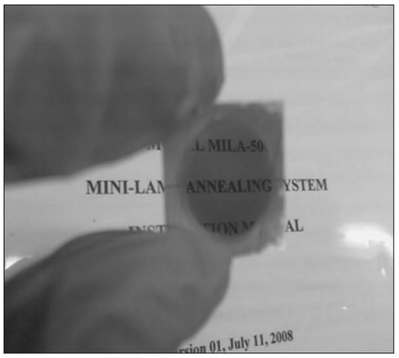

(d)

Figure 1. ESEM microphotographs of frontal view of porous alumina template: a) before and b) after barrier removal; (c) SEM image of cross sectional view; d) photograph of as-anodized thin transparent template on ITO/glass substrate.

The barrier layer separating the substrate from the pore channel being etched away can offer a straightforward method toward the fabrication of nanostructured arrays. Figure 1b shows the PAA after the barrier oxide removal process which served as a widening treatment of the nanopore walls, as well. This resulted in highly ordered vertically aligned nanopores with an average diameter of 65 nm and an interpore spacing of about 100 nm. The aspect ratio of the fabricated nanopores ranged 3:1–20:1. A cross sectional view of the template from Figure 1c shows that the nanopores are straight, parallel and have smooth inner walls. The SEM images of the obtained anodic porous alumina films were processed using standard imaging software showing a porosity level of 60%, resulting in a pore density of 1.4×10^{10} pores cm^{-2}.

When aluminum is oxidized to alumina, there is a significant volume expansion. In our case, the expansion factor of 1.3 was considered after experimentally measuring the alumina thickness with a profiler and by taking into account the charge flow during the anodization process (density of aluminum was considered 2.7 g cm^{-3} and the porous alumina one 3.2 g cm^{-3}). Therefore, in all cases, the second anodization step was performed in order to produce a thin alumina film of 200 to 600 nm thickness.

Electrodeposition of ZnO is generally based on the generation of hydroxide ions (OH^-) at the surface of a conducting electrode by cathodic reduction of a precursor such as nitrate ions (NO^{3-})[25] or molecular oxygen (O_2).[18]

In the first studied electrolyte (A), $ZnCl_2$ was employed as zinc precursor and KCl as supporting electrolyte. Hydrogen peroxide was used as an oxygen precursor as it does not give rise to undesired reaction products. H_2O_2 is especially interesting because it presents a high solubility in water (up to 10 M) and, therefore, it allows achieving high deposition rates.[26]

As for equation 1, the reduction of hydrogen peroxide leads to the formation of hydroxide ions:

$$H_2O_2 + 2e^- \rightarrow 2OH^- \quad [1]$$

After OH^- ions are generated, they immediately precipitate in presence of Zn^{2+} to form $Zn(OH)_2$ which is easily dehydrated at 80°C to form ZnO. Therefore, the reaction of ZnO deposition in the presence of H_2O_2 can be written as:

$$Zn^{2+} + 2OH^- \rightarrow ZnO + H_2O \quad [2]$$

The process leads to a pH increase and to a local supersaturation of the solution in the vicinity of the electrode which provokes the precipitation on the electrode surface of amorphous ZnO.[27] Therefore, the electrolyte based on $ZnCl_2$ salt (electrolyte A) consisted in 5 mM $ZnCl_2$, 0.1 M KCl and 5 mM H_2O_2 and the pH was adjusted to 6.4. In case of electrolyte A, the nanorods were obtained by PED under a potential controlled mode with an intermittent symmetric square pulse. It is known that in aqueous deposition solutions, the high cathodic potentials cause some hydrogen evolution which can prevent the deposition. Hence, the delay time between pulses in the PED will compensate for the slow diffusion driven transport of Zn^{2+} into the pores, improving the filling factor of the holes, and consequently, the density of the nanorods in the AAO membranes. The pulsed deposition was carried out between −1.1 V and the open circuit potential. The on time was 0.25 sec and the off time was always maintained at 0.5 sec. The pulses were supplied up in order to reach the cathodic charge necessary to fill the template pores.

Further, nitrate ions were employed as zinc precursor (electrolyte B consisting in 0.01 M $Zn(NO_3)_2$). The growth mechanism of the ZnO nanowire arrays into the alumina template could be explained as follows. From the viewpoint of chemical reactions, the electrochemical deposition reactions to prepare ZnO film are proposed as[25]:

$$Zn(NO_3)_2 \rightarrow Zn^{2+} + 2NO_{3^-} \quad [3]$$

$$NO_{3^-} + H_2O + 2e^- \rightarrow NO_{2^-} + 2OH^- \quad [4]$$

$$Zn^{2+} + 2HO^- \rightarrow Zn(OH)_2 \quad [5]$$

$$Zn(OH)_2 \rightarrow ZnO + H_2O \quad [6]$$

The OH^- ions obtained from the reduction of the nitrate ions increase the local pH on the electrode surface thus it is an important aspect to be controlled and adjusted.[28] The deposited $Zn(OH)_2$ is subsequently decomposed and form ZnO on the substrate.

In order to have a more stabilized system, 0.1 M H_3BO_3 was added to $Zn(NO_3)_2$ (electrolyte C). Further, the electrodeposition of the nanorods was studied by applying a constant potential of −1.1 V for up to 30 minutes.

Higher deposition temperature can be used in non-aqueous baths, which usually leads to higher crystallinity. For this reason, a non-aqueous DMSO solution of 0.1 M $Zn(NO_3)_2$ (electrolyte D) was employed. The electrodeposition was performed either under constant potential of −1 V or by pulsed potential deposition when time on and time off values were the same used in case of electrolyte A.

The theoretical electrical charge value, Q_{th}, to fill the alumina template was estimated by the following equation 7:

$$Q_{th} = zF\rho h A_{eff}/M.M. \quad [7]$$

where z is the number of exchanged electrons (2), F is the Faraday constant (96487 C mol^{-1}), ρ is the density of the deposited material (g cm^{-3}), h is the alumina thickness (cm) and A_{eff} represents the effective area of nanopores (cm^2). The A_{eff} value is given by eq. 8:

$$A_{eff} = PxA \quad [8]$$

where A is the alumina exposed area (cm^2) and P is the porosity (%).

A preliminary study of the optimal electrodeposition parameters was performed by cyclic voltammetry at a 20 mV s^{-1} sweep rate. From the I-E characteristics, the ZnO deposition was associated with a potential around −1 V in all the electrolytes used for the nanorods synthesis into the thin alumina template. The electroreduction of the oxygen species generated hydroxide ions at the cathode. The potential at zero current was close to −0.2 V, value characteristic to the Zn^{2+}/Zn system. The steep increase in the cathodic current starting from −1.2 V corresponded to zinc deposition which is further reoxidized during the reverse sweep starting −0.2 V. Therefore, in accordance with the corresponding ciclovoltammogram, an optimum value of the deposition potential within the potential window from −0.2 to −1.2 V was employed for each electrolyte studied for ZnO synthesis.

In order to follow the synthesis process, the current transients were recorded. Generally, the deposition process presents four stages (as marked in Figure 2). In the first stage, a sharp increase of the cathodic current (associated to the charge of the double layer) is observed when the voltage is applied; this is followed by the reduction of the Zn^{2+} ions located at the surface and the formation of a diffusion layer resulting in a current decrease. In the second stage – the growth of the nanorods – the current is nearly constant but once they reach the top surface, caps are formed at the top of nanorods and the current increases (stage three). The caps at top of nanorods start to coalescence in the fourth stage resulting in a film.

As an exemple, only the I-t transients recorded for 30 minutes for the growth of the ZnO into the alumina nanopores from an aqueous solution and non-aqueous solution are presented in Figures 2a and 2b. As one can see, in particular in the case of DMSO solution, all stages are reached. The diffusion layer that normally appears after the reduction of zinc ions located at the electrode surface is formed more slowly in the aqueous solution due to the poor diffusion of species toward the electrode. Therefore, the second stage of growth is reached almost twice slower in the aqueous solution C and for the same deposition time the top of nanorods are caps-free in this case. The SEM image in Figure 3a confirms the presence of the caps that started to coalescence at the top of nanorods obtained in the DMSO based electrolyte.

In order to gain a further insight into the growth mechanism of the nanorods from the chosen electrolytes, a detailed study of the evolution of the nanorod dimensions as a function of the charge (i.e. time of deposition) was performed. It has been observed that the length of the obtained nanorods was higher in the case of DMSO, by a factor

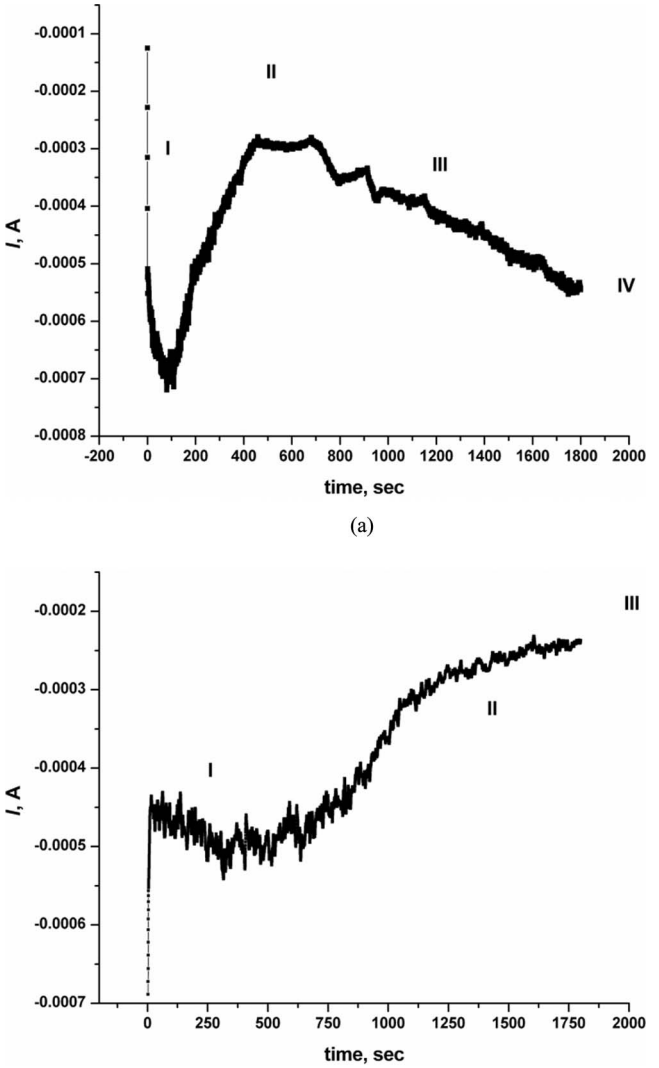

Figure 2. Chronoamperometric curves recorded under constant potential of −1 V for the growth of ZnO NR a) solution D and b) solution C.

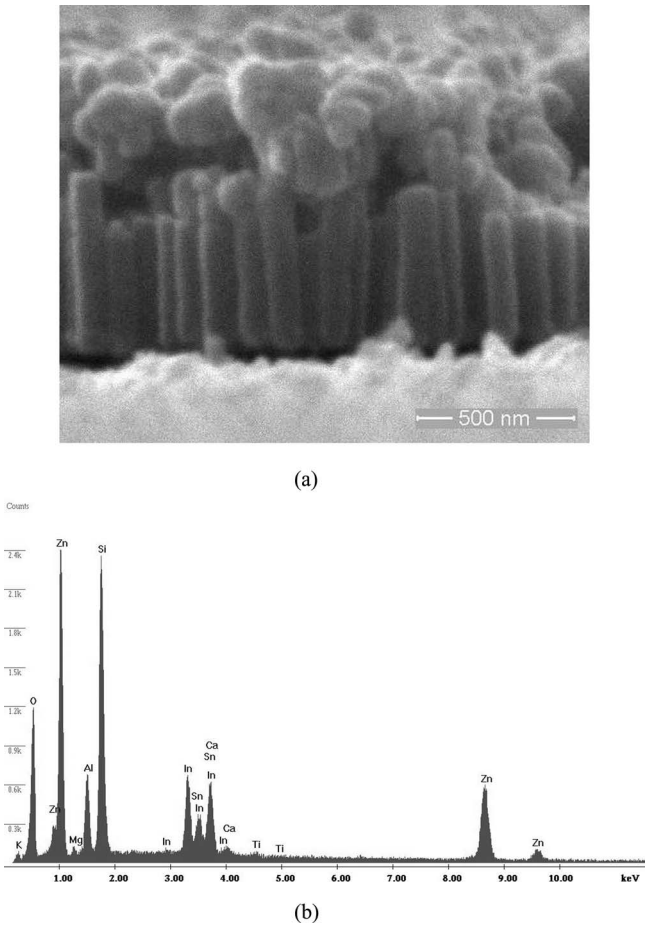

Figure 3. a) SEM images of the ZnO NR electrodeposited into thin alumina template by potentiostatic method in 0.1 M $Zn(NO_3)_2$ in DMSO and b) corresponding EDAX spectrum.

of 2.5, demonstrating the higher wettability and ionic mobility within the thin PAA template used in non-aqueous media with respect to aqueous one.

The efficiency of the deposition was calculated from the ratio Q_{exp}/Q_{th} (%) for ZnO NR, where Q_{exp} and Q_{th} are the experimental and theoretical exchanged quantity of electricity, considering a current efficiency of 100%. In case of aqueous electrolytes A and B, a value of 35–40% efficiency was obtained and slightly improved to 45% when H_3BO_3 was added (solution C). In DMSO, a value of 50% efficiency was obtained for the potentiostatic deposition and up to 65% in the case of pulsed deposition method. These values prove incomplete filling of all the pores of the template due to its small pore size. Another possible explanation for the efficiency values obtained could result from pore to pore variations in the cathode interface, which may have an influence on the nucleation rate. Either the presence of very small amounts of adsorbed impurities or the heterogeneities caused by grain boundaries could completely suppress the nucleation of a wire. Prieto et al.[29] tried to explain similar difficulties in template-growing of nanowires when only 10–20% filling efficiency was reached.

Nevertheless, this work reports for the first time the highest efficiency deposition of c-axis oriented ZnO NR grown in thin PAA templates supported on ITO/glass by employing DMSO as supporting electrolyte. The electrolyte D based on 0.1 M $Zn(NO)_3$ in DMSO and the chosen deposition parameters favor the ZnO NR deposition yielding the highest value reported till now in the matter.[30]

SEM image of the ZnO NR obtained in stage IV of growth in organic media is presented in Figure 3a, after a partial dissolution of the alumina template. It is obvious from here that the ZnO NR growth followed the aspect ratio of the template used for the deposition. The non-homogeneous length of the nanorods may be indicative of differences in the nucleation time from pore to pore due to interfacial structure differences between them. In Figure 3a, the nanorods followed a coalescence process and formed a porous film on top of template. It can be seen, as well, that the uniformly distributed ZnO NR are smooth and present a mean diameter of 65 nm which is consistent with the original pore diameter of the template. Some nanorods were broken off and even stripped off from the pores of the template due to the mechanical forces during cleaving.

EDAX measurements regarding the electrodeposition of ZnO NR into the PAA template in both aqueous and organic media are shown in Figure 3b and confirm the obtaining of ZnO since Zn, O and trace amounts of ITO substrate and PAA template were present in all the samples.

Nanorods aspect ratio depends on the nuclei sizes, density and preferential orientation. The X-ray diffraction patterns of PAA template/ITO substrate before and after synthesis of ZnO NR arrays from aqueous and organic media are shown in Figure 4. The XRD measurements showed aside to the diffraction peaks of the substrate materials, the ones of the ZnO material. Strong reflections corresponding to (100), (002) and (101) planes of ZnO were observed. As a general rule,

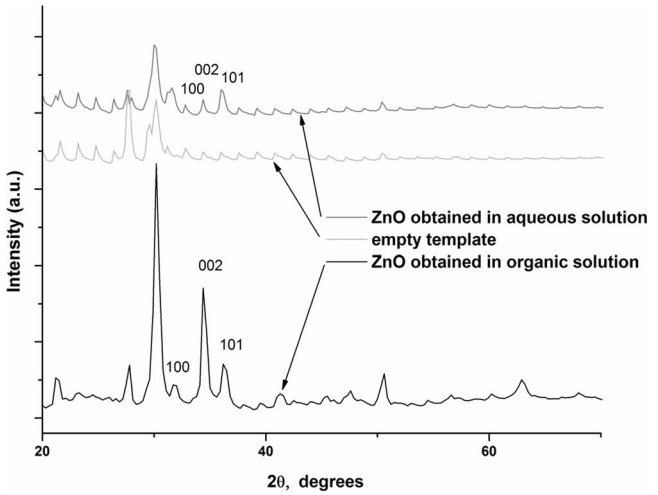

Figure 4. XRD pattern of the ZnO nanowire arrays embedded in the alumina template/ITO substrate.

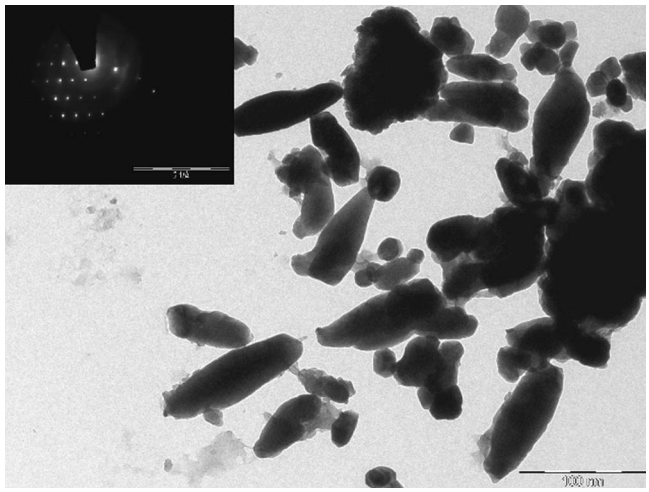

Figure 5. TEM images of ZnO NR detached by etching from the PAA template and corresponding selected-area electron diffraction pattern.

the diffraction peaks are very narrow, revealing the good crystalline character of the samples. Furthermore, it is clear from Figure 4 that the ZnO NRs exhibit no obvious preferred orientation when synthesized in aqueous media. It has been suggested that the different orientation growth is induced by defects in the wall of the template pores, such micro twins, stacking faults, and low-angle grain boundaries.[31]

On the other hand, in the organic electrolyte, it was evident that the (002) reflections at 2θ of 35° were of maximum intensity, indicating thereby a strong orientation with stacking of the planes along the c-axis, meaning that the velocity of crystal growth along c-axis was higher than for other directions. With respect to the background, the peak intensity demonstrates the high purity of the hexagonal ZnO phase and good crystallinity of the samples.

The mean grain size can be evaluated by using the Debye-Scherrer relation:

$$B = 0.9\lambda/t\ \cos\theta \qquad [9]$$

where B is fwhm (full width at half maximum) of the broadened diffraction line on the 2θ scale, t is diameter of the crystallites, λ - the wavelength of the X-ray radiation and θ – the Bragg angle.[32]

Evaluation of the (002) diffraction peak using the Debye-Scherrer formula revealed that the mean grain size of ZnO NR was about 20 nm. The increase in preferred orientation is attributed to the increased number of grains along the plane. This implies that more Zn^{2+} ions are converted into ZnO NR with predominant longitudinal growth. Due to the highest growth rate of the ZnO (002) plane, the ZnO nuclei quickly elongate along the c-axis direction and only those ZnO nuclei with c-axis direction parallel to the substrate surface normal have the chance to grow due to limited in-plane space. Hence, a well-aligned ZnO nanorod array is formed. Owing to the minimum surface free energy of the (002) plane, the (002) direction of a ZnO thin film is the most thermodynamically favorable growth direction.[33] This is the intrinsic factor leading to ZnO crystals preferentially growing along the c-axis orientation while the growth conditions represent the extrinsic factors.

Taking into account the results obtained and the setup parameters, it can be concluded that the use of an organic electrolyte type DMSO for an increased diffusion of Zn^{2+} ions toward the cathode in order to react with OH^- ions is of paramount importance for the growth of nanorods along c-axis. This is a major result that allows obtaining ZnO NR by electrodeposition which presents a big advantage in comparison to other techniques generally resulting in lateral growth.

As Redón et al.[21] showed, the PAA surfaces interact with liquid phases via surface groups, thus, the polar component partially defines the strength of the interaction between the liquid and the PAA surface.[34] Water exhibits high values of the dielectric constant (ε_r) and dipole moment (μ), but it also has the highest value of the surface tension (γ) which prevents water from spreading and filling the pores to afford high equilibrium contact angle (θ_{eq}) values and so results in a worse hydrogen bond interaction with the hydroxide groups from the PAA surface with respect to DMSO which has higher values of ε_r and μ, but lower γ and therefore a higher wetting force. Organic materials and most solvents are considered as low energy materials with respect to their surface energies, whereas inorganic materials are referred as high energy materials (covalent, ionic and metallic). Low energy liquids spread rapidly on high energy surfaces. If the adhesive force solid-liquid (γ_{sl}) is strong enough to overcome the cohesive force liquid-vapor (γ_{lv}), the pores will be completely filled as in the case of DMSO which proved to have the perfect equilibrium between polar and surface tension properties for a complete filling of the porous surface. These findings showed the convenience for using DMSO as solvent to facilitate the filling of the porous alumina template.

We studied the growth of the vertically aligned nanorods since they are a promising solution to increase the efficiency of solar cells in terms of the fast electron transportation due to the fact that the c-axis orientation represents the highest electronic density path (for electrons) to be conducted along and thus, to be collected efficiently.[35] Moreover, nowadays new fields are emerging such as coupling of semiconductor with photon excitation process that could form the field of opto-electronics, and so, additional effects could be proposed by coupling semiconductor with piezoelectric to form a field of piezotronics, and piezoelectric with photon excitation to form a field of piezophotonics. Furthermore, a coupling among semiconductor, photon excitation and piezoelectric gives the field of piezo-phototronics,[36] which can be the basis for fabricating piezo-photonic/electronic nanodevices.

The general TEM image of some ZnO NR deposited from DMSO electrolyte after partial dissolution of PAA template, (Figure 5) shows that the diameter size is homogeneous from one wire to another, but at the same time it differs along the nanowire length. The reason for exhibiting this morphology is probably due to the etching process in the NaOH solution used to free them; even if the pH of solution used to dissolve the PAA template is slightly above 9, a slow process of etching takes place at the ends of the nanorods, as showed by Jun Zhou et al.[37] Moreover, as He et al. presented, the edges of ZnO NR are etched by NaOH solution of pH 9, the etching depth being lower as the pH of the solution is decreasing toward 7.[38] Adjusting the etching time to be long enough for efficient template removal seems to have detrimental effects on the ZnO NR. To date, the controllable wet chemical etching to remove partial PAA template is rare in the literature. A compromise should be found between the two etching processes. Because of the full solubility of ZnO_2^{2-}, the etching of the

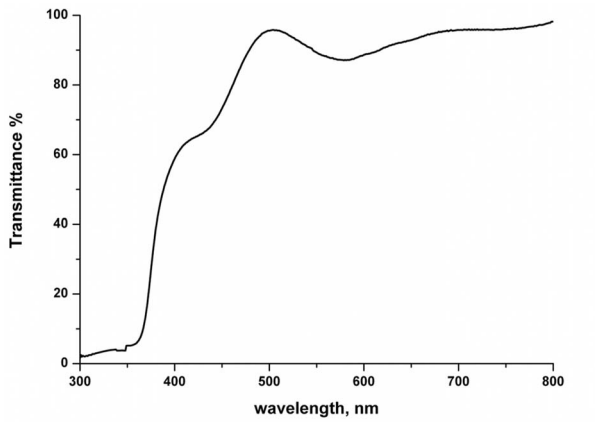

Figure 6. Transmittance spectra of ZnO NR synthesized in DMSO (electrolyte D).

ZnO by NaOH solution can be attributed to the chemical process:

$$ZnO(s) + 2OH^- \rightarrow ZnO_2^{2-} + H_2O \quad [10]$$

From the selected-area electron diffraction (SAED) pattern of ZnO NR corresponding to hexagonal wurzite ZnO (inset of Figure 5) it is noted that the diffraction rings are discontinuous and consist of rather sharp spots, which indicates well crystallization of the nanorods. These results confirmed that the ZnO NR electrodeposited in ultrathin PAA templates were single crystal in nature.

Figure 6 shows the UV–visible absorption spectrum for the ZnO NRs after 300°C annealing. Measurements were taken in the wavelength range 300–1100 nm on the templates before and after deposition. The deposited ZnO NRs were highly transparent in the visible-light range (mean transmittance 80%) and absorption onset at around 350 nm, close to the expected position of ZnO direct band edge absorption. The transmittance at the short-wavelength limit (350 nm) is not null indicating that the coverage of the PAA/substrate system with the nanorods is not complete, and therefore, the bandgap could not be obtained accurately from the transmittance data.

For the electrical resistivity measurement, the ZnO NR were left embedded in the template and two leads were fixed on the ITO layer and the Au layer sputtered on the caps grown on top of the wires (Figure 7). Macrocontact measurements are 2-point contact measurements, and an effort is required to eliminate the contact resistance contribution. This can be achieved by using differently sized contact pads. For an array of 4×10^8 nanorods (theoretical number) of 60 nm diameter and long about 500 nm grown in an alumina template with 60% porosity, one arrives at a theoretical parallel resistance of the nanowire array of 5–10 Ω or at a theoretical value of 3500 Ω cm, respectively, considering an average current efficiency of 50% and a resistivity of 390 Ω cm as Jr H. He et al.[38] found for a single ZnO nanorod. The high electrical resistivity in a single undoped ZnO nanorod is indicative of its high quality of crystalline structure with low oxygen deficiencies. The resistance of the leads does not affect the measurement but since the exact number of contacted nanorods is unknown, absolute values of the electrical resistivity cannot be determined in the case of arrays.[39] Our parallel resistance values ranged 20 Ω (for nanorods grown in DMSO under pulsed potential electrodeposition) to 100 Ω (for nanorods grown in organic media under potentiostatic electrodeposition). An explanation of these values could come from considering the inhomogeneity in the nanorod growth, which results in only part of them being contacted.[40] During electrodeposition, the concentration of Zn ions at the cathode interfaces decreases with reaction time, but this problem can be improved in pulsed electrodeposition. This is because the relaxation time plays an important role in the recovery and redistribution of the metal ion concentration at the deposition interface during the off-time.[41] In addition, the relaxation time limits the hydrogen evolution occurring at the surface of PAA during electrodeposition. Besides the inhomogeneity in nanowire growth, the contact resistance contribution has to be taken into account. Thin Ti and W layers have to be considered for the measurement as they may influence the contact between the nanorods and the substrate. Although 2-point measurement has the great advantage of requiring no special equipment and no long and expensive lithographic procedures, its geometry is inherently limiting in that the number of nanorods contributing to the conduction is unknown. Unambiguous values for the resistivity, as well as for certain other transport properties, can only be reliably obtained by performing conductive atomic force microscopy measurements on individual nanorods. The work on this matter is ongoing.

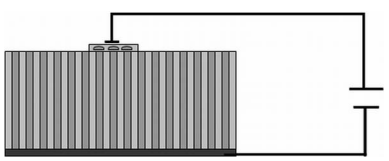

Figure 7. Scheme of 2-point measurement of ZnO NR embedded in alumina templates.

Conclusions

The present work demonstrates the fabrication of uniform ZnO nanorods with a mean diameter consistent with the original nanopores of the prefabricated alumina templates. A 60% deposition efficiency was measured here when single crystalline c-axis oriented ZnO nanorod arrays were electro-synthesized in DMSO-based electrolyte, a value never reported so far in the field.

By a fine adjustment of the ZnO deposition conditions (appropriate concentrations of the zinc precursor, deposition potential, temperature, etc.) and the parameters employed to fabricate the ultra-thin PAA templates, a full control of the crystallographic orientation of the ZnO nanorods along with their morphology was achieved.

Both template quality and the use of DMSO as electrolyte were found of having paramount importance for the results achieved. As a conclusion, it is here reported a method demonstrating that a high yield synthesis of uniform ZnO nanorods characterized by a constrained crystallographic direction can be obtained by direct template electrodeposition at low temperatures without any post-annealing treatment, and with a nanorod length of the order of a few hundred nanometers allowing the proper operation of organic optoelectronic devices.

Acknowledgments

The authors thank for the financial support by the European Commission, DG Research through the program PEOPLE, by the project no. MRTN-CT-2006-035884.

References

1. S. Bandyopadhyay and A. E. Miller, in *Handbook of Advanced Electronic and Photonic Materials and Devices*, Editor: H. S. Nalwa, Academic, San Diego (2000).
2. K. Nomura, H. Ohta, K. Ueda, T. Kamiya, M. Hirano, and H. Hosono, *Science*, **300**, 1269 (2003).
3. R. Könenkamp, R. C. Word, and C. Schlegel, *Appl. Phys. Lett.*, **85**, 6004 (2004).
4. M. S. Wagh, L. A. Patil, T. Seth, and D. P. Amalnerkar, *Mater. Chem. Phys.*, **84**, 228 (2004).
5. S. J. Pearton, W. H. Heo, M. Ivill, D. P. Norton, and T. Steiner, *Semicond. Sci. Technol.*, **19**, R59 (2004).
6. H. Zhou and Z. Li, *Mater. Chem. Phys.*, **89**, 326 (2005).
7. H. Zhang, D. Yang, X. Ma, Y. Ji, J. Xu, and D. Que, *Nanotechnology*, **15**, 622 (2004).
8. P.-A. Hu, Y.-Q. Liu, L. Fu, X.-B. Wang, and D.-B. Zhu, *Appl. Phys. A*, **78**, 15 (2004).
9. J. Sh. Jie, G. Zh. Wang, Y. M. Chen, X. H. Han, Q. T. Wang, B. Xu, and J. G. Hou *Appl. Phys. Lett.*, **86**, 031909 (2005).
10. M. H. Huang, S. Mao, H. Feick, H. Q. Yan, Y. Y. Wu, H. Kind, E. Weber, R. Russo, and P. D. Yang, *Science*, **292**, 1897 (2002).
11. W. I. Park and G. Ch. Yi, *Adv. Mater.*, **16**, 87 (2004).
12. V. Branzoi, F. Branzoi, and L. Pilan, *Mat. Chem. Phys.*, **118**, 197 (2009).

13. M. Ionită and A. Prună, *Prog. Org. Coat.*, **72**, 647 (2011).
14. V. Brânzoi, A. Prună, and F. Brânzoi, *Mol. Cryst. Liq. Cryst.*, **485**, 853 (2008).
15. Y. Li, G. W. Meng, L. D. Zhang, and F. Phillip, *Appl. Phys. Lett.*, **76**, 2011 (2002).
16. A. Prună, V. Brânzoi, and F. Brânzoi, *J. Appl. Electrochem.*, **41**, 77 (2011).
17. H. Zhou, H. Alves, D. M. Hofmann, W. Kriegseis, and B. K. Meyer, *Appl. Phys. Lett.*, **80**, 210 (2002).
18. S. Peulon and D. Lincot, *J. Electrochem. Soc.*, **145**, 864 (1998).
19. Q. Wang, G. Wang, B. Xu, J. Jie, X. Han, G. Li, Q. Li, and J. G. Hou, *Mater. Lett.*, **59**, 1378 (2005).
20. D. Gal, G. Hodes, D. Lincot, and H. W. Schock, *Thin Solid Films*, **361–362**, 72 (2000).
21. R. Redón, A. Vázquez-Olmos, M. E. Mata-Zamora, A. Ordóñez-Medrano, F. Rivera-Torres, and J. M. Saniger, *J. Colloid Interface Sci.*, **287**, 664 (2005).
22. Y. L. Lee and C. H. Chang, *J. Power Sources*, **185**, 584 (2008).
23. K. P. Musselman, G. J. Mulholland, A. P. Robinson, L. Schmidt-Mende, and J. L. MacManus-Driscoll, *Adv. Mater.*, **20**, 4470 (2008).
24. D. Ramirez, T. Pauporte, H. Gomez, and D. Lincot, *Phys. Stat. Sol. (A)*, **205**, 2371 (2008).
25. M. Izaki and T. Omi, *J. Electrochem. Soc.*, **143**, L53 (1996).
26. Th. Pauporté and D. Lincot, *J. Electrochem. Soc.*, **148**, C310 (2001).
27. M. Izaki, *J. Electrochem. Soc.*, **146**, 4517 (1999).
28. B. Q. Cao, W. P. Cai, F. Q. Sun, Y. Li, Y. Lei, and L. D. Zhang, *Chem. Commun.*, **14**, 1604 (2004).
29. A. Prieto, M. Sander, M. Martin-Gonzalez, R. Gronsky, T. Sands, and A. Stacy, *J. Am. Chem. Soc.*, **123**, 7160 (2001).
30. R. Tena-Zaera, J. Elias, C. Lévy-Clément, I. Mora-Seró, Y. Luo, and J. Bisquert, *Phys. Stat. Sol. (A)*, **205**, 2345 (2008).
31. M. J. Zheng, L. D. Zhang, G. H. Li, and W. Z. Shen, *Chem. Phys. Lett.*, **363**, 123 (2002).
32. B. D. Cullity and S. R. Stock, in *Elements of X-ray Diffraction*, 3rd Ed Prentice-Hall, Inc, chapter 14 (2001).
33. N. Fujimura, T. Nishihara, S. Goto, J. Xu, and T. Ito, *J. Cryst. Growth*, **130**, 269 (1993).
34. O. K. Varghese, D. Gong, M. Paulose, K. G. Ong, C. A. Grimes, and E. C. Dickey, *J. Mater. Res.*, **17**, 1162 (2002).
35. L. Vayssieres, *Adv. Mater.*, **15**, 464 (2003).
36. Y. F. Hu, Y. L. Chang, P. Fei, R. L. Snyder, and Z. L. Wang, *ACS Nano*, **4**, 1234 (2010).
37. J. Zhou, N. G Xu, and Z. L. Wang, *Adv. Mater.*, **18**, 2432 (2006).
38. H. He Jr, C. S. Lao, L. J. Chen, D. Davidovic, and Z. L. Wang, *J. Am. Chem. Soc.*, **127**, 16376 (2005).
39. Q. H. Li, Q. Wan, Y. X. Liang, and T. H. Wang, *Appl. Phys. Lett.*, **84**, 4556 (2004).
40. J. Lee, S. Farhangfar, J. Lee, L. Cagnon, R. Scholz, U. Gösele, and K. Nielsch, *Nanotechnology*, **19**, 365701 (2008).
41. D. Pullini and D. Busquets, *ACS Appl. Mater. Interfaces*, **3**, 759 (2011).